Applied Physics Letters

Anomalous lasing of high-speed 850 nm InGaAlAs oxide-confined vertical-cavity surface-emitting lasers with a large negative gain-to-cavity wavelength detuning

Cite as: Appl. Phys. Lett. **105**, 061104 (2014); https://doi.org/10.1063/1.4892885
Submitted: 27 February 2014 • Accepted: 31 July 2014 • Published Online: 11 August 2014

S. A. Blokhin, M. A. Bobrov, N. A. Maleev, et al.

Anomalous lasing of high-speed 850 nm InGaAlAs oxide-confined vertical-cavity surface-emitting lasers with a large negative gain-to-cavity wavelength detuning

S. A. Blokhin,[1,a)] M. A. Bobrov,[1] N. A. Maleev,[1] A. G. Kuzmenkov,[2,1] A. V. Sakharov,[1] A. A. Blokhin,[3] P. Moser,[4] J. A. Lott,[4] D. Bimberg,[4,5] and V. M. Ustinov[1]
[1]*A. F. Ioffe Physical-Technical Institute of the Russian Academy of Sciences, 26 Polytekhnicheskaya Street, Saint Petersburg 194021, Russian Federation*
[2]*Submicron Heterostructures for Microelectronics, Research and Engineering Center of the Russian Academy of Sciences, 26 Polytekhnicheskaya Street, Saint Petersburg 194021, Russian Federation*
[3]*Saint Petersburg State Polytechnical University, 29 Polytekhnicheskaya Street, Saint Petersburg 195251, Russian Federation*
[4]*Zentrum für Nanophotonik, Technische Universität Berlin, Hardenbergstrasse 36, Berlin 10623, Federal Republic of Germany*
[5]*Electric and Computer Engineering Department, King Abdul-Aziz University, Jeddah 21589, Kingdom of Saudi Arabia*

(Received 27 February 2014; accepted 31 July 2014; published online 11 August 2014)

The impact of a large negative quantum well gain-to-cavity etalon wavelength detuning on the static and dynamic characteristics of 850 nm InGaAlAs high-speed oxide-confined vertical-cavity surface-emitting lasers (VCSELs) was investigated. Three distinct lasing regimes were revealed in large square aperture (≥ 7 μm per side) devices with large detuning including: (1) an anomalous lasing via higher order Hermite–Gaussian modes at low forward bias current; (2) lasing via the lowest order Hermite–Gaussian modes at high bias current; and (3) simultaneous lasing via both types of transverse modes at intermediate bias currents. In contrast to conventional multimode VCSELs a two-resonance modulation response was observed for the case of co-lasing via multiple transverse modes with high spectral separation. The reduction in the oxide aperture area resulted in classical lasing via the lowest order modes with a conventional single-resonance frequency response. [http://dx.doi.org/10.1063/1.4892885]

Vertical-cavity surface-emitting lasers (VCSELs) based on the InGaAlAs-materials system on GaAs substrates are the most pervasive among all semiconductor laser diode types used in modern high-bit rate (>10 Gbit/s) short-reach and medium-reach optical data communication systems and high-performance computing systems.[1] The drastically growing demand for data communications bandwidth, energy efficiency, and cloud storage capacity via fiber-optic cables to and from data centers is one of the biggest technical challenges of our day. The same attributes are critical for very-short-reach (<1 m) optical interconnects (OIs) as well, such as the VCSEL-based interchip, board-to-board, and server-to-server OIs employed in supercomputers. The most prevalent solution for this problem is to increase the per-lane data rate of the transceiver optical subassembly modules and to use parallel optical lanes. To improve the high-speed VCSEL performance under direct current modulation at 850 nm, the most recent design changes that seek to optimize device performance include the use of multiple thin $In_yGa_{1-y}As$ (with $y \sim 0.08$) quantum wells (QWs) with $Al_xGa_{1-x}As$ barrier layers (with $x \sim 0.3$–0.5), multiple selectively oxidized $Al_xGa_{1-x}As$ current, mode-shaping, and capacitance-reducing oxide aperture layers (with $x \sim 0.95$–0.98), and the construction of these VCSELs in practical high bit rate geometries using planar high frequency (HF) transmission line contact pads on planarizing spin-on dielectric material to reduce the intrinsic contact pad capacitance.[2] A proper spectral misalignment between the cavity fundamental resonance (Fabry-Perot etalon) wavelength and the spectral gain maximum wavelength of the QW active region (the gain-to-cavity wavelength detuning) is widely used to improve a VCSEL's static characteristics such as the power conversion efficiency and the temperature stability.[3] The influence of the gain-to-cavity detuning on the VCSEL's dynamic characteristics is of great interest as well. In this Letter, we analyze the static and dynamic characteristics of 850 nm high-bit rate VCSELs with an unusually large (>20 nm) spectral gain-to-cavity detuning.

Traditional high bit rate top-emitting VCSELs with fully doped all-semiconductor distributed Bragg reflectors (DBRs) were selected as the basis for our 850 nm VCSEL study. The epitaxial structures were grown on undoped {001}-oriented 2° off toward the nearest ⟨110⟩ GaAs substrates by metal-organic vapor-phase epitaxy, and consist of an ~59 nm-thick p+-doped GaAs ohmic contact layer, a top $Al_{0.1}Ga_{0.9}As$/$Al_{0.9}Ga_{0.1}As$ p-doped DBR (23 periods) with two ~30 nm-thick $Al_{0.98}Ga_{0.02}As$/$Al_{0.9}Ga_{0.1}As$ aperture layers in the first two low-index layers adjacent to the microcavity, a 1.0λ-thick AlGaAs microcavity with five ~4 nm-thick strained $In_{0.08}Ga_{0.92}As$ QWs surrounded by 6-nm-thick $Al_{0.45}Ga_{0.55}As$ barrier layers, a bottom $Al_{0.15}Ga_{0.85}As$/$Al_{0.9}Ga_{0.1}As$ n-doped DBR (35.5 period), and a 1.5 μm-thick n+-doped GaAs ohmic contact buffer layer above the substrate. To enhance our high-speed VCSEL performance the epitaxial structure parameters were tuned including a proper energy band

a)Electronic mail: blokh@mail.ioffe.ru

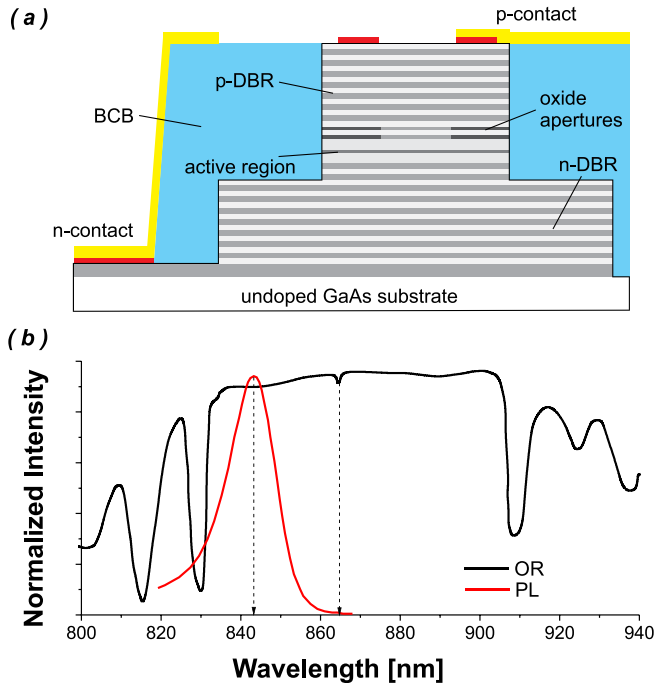

FIG. 1. Oxide-confined 850-nm QW InGaAlAs VCSEL: (a) Schematic cross-sectional view; (b) PL of a QW test wafer and OR spectra of the VCSEL wafer both at 25 °C. The black dash arrows indicate the PL peak and the cavity resonance.

structure of the strained quantum-well InAlGaAs active region, DBR modulation doping to obtain a low series resistance and low internal optical losses, and the use of multiple oxide layers to achieve a small VCSEL mesa capacitance.[4] Post-growth processing included contact photolithography, dry etching, selective wet oxidation of the high AlAs mole-fraction AlGaAs layers, vacuum e-beam p- and n-contact metal deposition, planarization using a thick dry-etch BCB layer, and Ti/Pt/Au contact pad metallization. Photomasks were designed such that sets of adjacent VCSELs with square oxide aperture edge dimensions of from 0 μm to 8 μm were formed in one fabrication process. The schematic cross-section of the processed oxide-confined 850 nm VCSEL is shown in Figure 1(a). Note that the room temperature photoluminescence (PL) peak for a laser-pumped QW calibration epitaxial wafer grown just before the full VCSEL is at 843 nm with a full wafer variation of $\leq$2 nm. The wavelength of the VCSEL etalon measured by optical reflectance (OR) is at $\sim$865 nm at wafer center (and $\sim$870 nm near the wafer edges), which corresponds to a negative gain-to-cavity detuning of 22 nm at wafer center as shown in Figure 1(b). To estimate the real gain-to-etalon cavity wavelength detuning for a given VCSEL, the emission spectrum below the threshold current was measured.

Figure 2(a) shows typical continuous wave (CW) light output power-current-voltage (L-I-V) characteristics for the square aperture oxide-confined 850 nm VCSELs with a negative gain-to-cavity detuning of more than 20 nm. The devices with oxide aperture square sides of 6 μm or less have smooth light-current (L-I) curves similar to the conventional oxide-confined 850 nm VCSELs with a more typical $\sim$10 nm negative gain-to-cavity detuning.[4] At the same time, the L-I curves for our 850 nm VCSELs with oxide aperture square

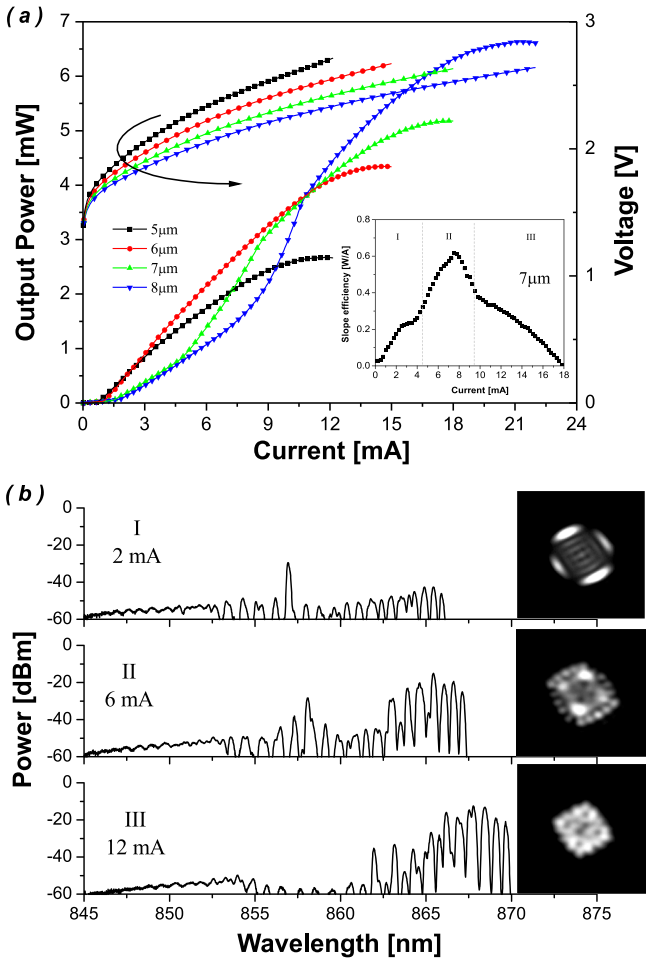

FIG. 2. Light output power-current-voltage (L-I-V) characteristics (a) and emission spectra and near-field intensity patterns (b) of oxide-confined 850 nm InGaAlAs QW VCSELs with a large $\sim$20 nm gain-to-cavity wavelength detuning. Inset in (a): slope efficiency as function of bias current for a 7 μm $\times$ 7 μm square oxide-confined VCSEL.

sides of 7 and 8 μm shown in Figure 2(a) have an anomalous behavior (kinks or abrupt nonlinearities in the light-current curve) at intermediate forward currents. For example, the dependence of the L-I slope efficiency on current for a 7 μm $\times$ 7 μm square aperture VCSEL has three distinct regions (see the inset in Figure 2(a)): (1) a rapid increase and saturation at 0.23 W/A due to the appearance of lasing with a threshold current of 1.5 mA (current region I); (2) a quick switching to lasing with an L-I slope of 0.61 W/A (current region II); and (3) a monotonic decrease in the L-I slope due to overheating (current region III). Generally, the L-I slope efficiency of VCSELs is determined by injection efficiency, internal optical loss, and mirror loss.[2] The mirror loss is relatively insensitive to an increase in bias current due to the weak thermal dependence of the refractive index and the very small thermal expansion of the DBR layers. The I-V curves in Figure 2(a) are smooth and do not have kinks, hence, the injection efficiency is very stable with current. One can suppose that the observed behavior is due to drastic changes in the VCSEL mode structure since each cavity mode has an individual intrinsic optical loss therefore also its own individual lasing threshold current.

To clarify this situation, we recorded our VCSELs' lasing spectra and the near-field intensity patterns over their

entire operational current range. The oxide-confined 850 nm VCSELs with a large negative gain-to-cavity detuning and with oxide aperture square sides of 6 μm or smaller demonstrate classical lasing via low order transverse modes (not shown). However, as shown in Figure 2(b), the 7 μm × 7 μm square aperture oxide-confined VCSEL starts lasing at the wavelength of ~857 nm via a high-order Hermite–Gaussian mode (we call this the short-wavelength mode regime). However, the subsequent increase of bias current results in an increase of intensity of the lowest order Hermite–Gaussian modes (with a threshold of about 4.0–4.5 mA) and the simultaneous lasing via both types of transverse modes (we call this the two-state lasing regime). Finally, with additional forward bias current the lasing peaks at a root-mean-square emission wavelength of ~867 nm (we call this the long-wavelength mode regime). Note that a similar optical mode behavior was revealed for VCSELs with large aperture areas.

Anomalous switching from the high-order Laguerre–Gaussian mode lasing to the fundamental mode lasing was observed previously for 965 nm bottom-emitting VCSELs with a double oxide aperture.[5] Moreover, the low temperature studies of 960 nm broad-area top-emitting VCSELs with a single circular oxide aperture revealed a strong impact of the gain-to-cavity detuning on the transverse mode formation.[6] When the highest order modes are still well confined within the oxide aperture and the wavelengths of these highest order modes (and not the wavelengths of the lowest order modes) are close to the gain spectrum maximum, the VCSEL lasers on the highest order modes before the fundamental mode gain reaches its threshold. At higher currents self-heating results in a red shift of the active region gain spectrum and, thus, the gain available for the longer wavelength lowest order modes becomes higher. In the case of high material gain and low total internal loss, this effect can be observed in our VCSEL's even at room temperature.

To characterize the high-speed performance of our VCSELs with a large negative gain-to-cavity detuning, the small signal modulation response (S_{21}) and microwave reflection (S_{11}) were measured in the range from 50 MHz to 35 GHz. The dynamic physical parameters of our VCSELs were extracted by using a fitting procedure similar to that described in Ref. 4. Figure 3 shows the measured small signal modulation response curves at different forward bias currents for selected VCSELs. Note that the parasitic cut-off frequencies extracted from the S_{11} data are larger than 18 GHz over the entire current range and have a negligible impact on our VCSEL's high speed performance. As can be seen in Figure 3(a), the 5 μm × 5 μm square aperture oxide-confined VCSEL shows the classical single-resonance frequency response over its entire operating current range. However, as is clear from Figure 3(b), the situation is changed for our VCSELs with oxide aperture square sides of 7 μm. In current regions I and III, the devices exhibit the typical small-signal response for oxide-confined VCSELs.[4] In contrast, a two-resonance frequency response was revealed for the two-state lasing regime (current region II) with a low rate of increase of the modulation bandwidth with current. The square 8 μm × 8 μm aperture VCSELs demonstrate similar behavior (see Figure 3(c)). Table I summarizes the optical mode behavior and the small signal frequency response measured from oxide-confined

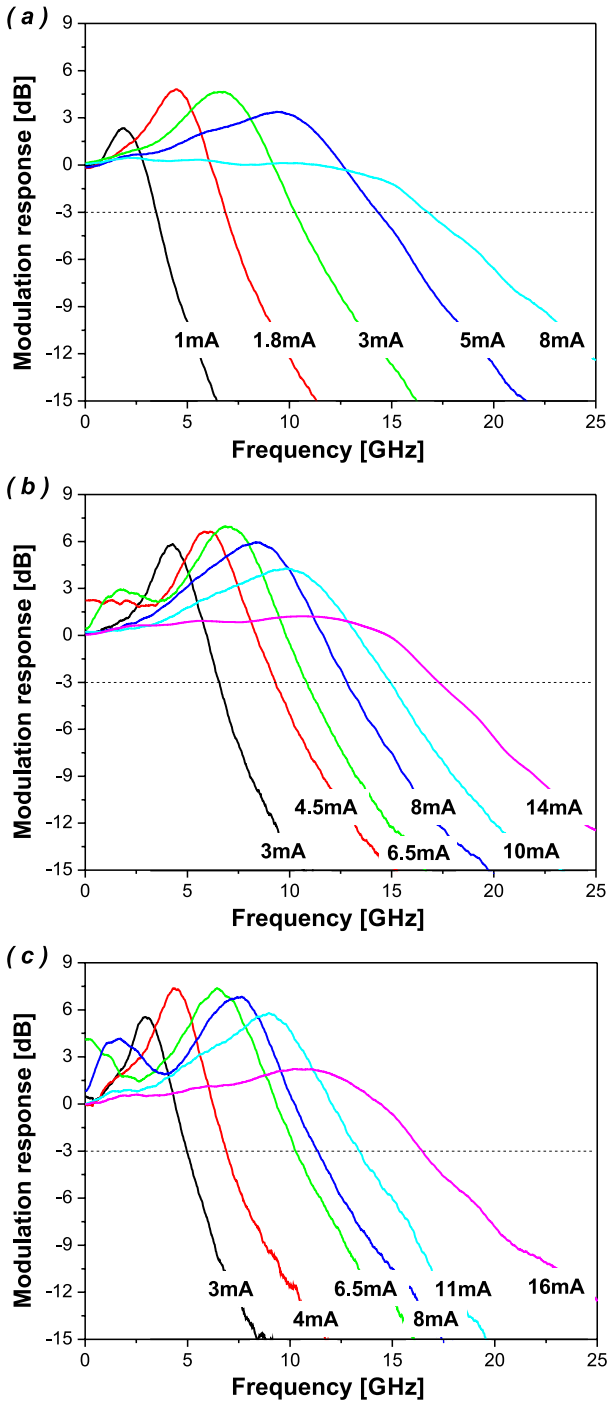

FIG. 3. Small signal modulation response S_{21} at different applied bias currents for 5 μm × 5 μm (a), 7 μm × 7 μm (b), and 8 μm × 8 μm (c) square oxide-confined 850-nm QW InGaAlAs VCSELs with a large ~20 nm gain-to-cavity detuning.

VCSELs with different gain-to-cavity wavelength detuning and different oxide aperture areas. We have investigated more than 10 devices for each oxide aperture size, and the static and dynamic characteristics were the same within the accuracy of our measurements.

Figure 4 shows the extracted −3 dB modulation frequency and the relaxation resonance frequency of 7 μm × 7 μm and 8 μm × 8 μm square aperture oxide-confined VCSELs as a function of bias current, where the conventional three-pole transfer function model can be applied. For the 7 μm × 7 μm square aperture oxide-confined VCSEL, the

TABLE I. Optical mode behavior and modulation response for selected oxide-confined VCSELs. T – ambient temperature, $\Delta\lambda$ – gain-to-cavity detuning, I_{th} – threshold current, λ_{low} – low mode wavelength above threshold current, λ_{high} – high mode wavelength above threshold current, n.a. – not available.

Aperture size (μm)	T (K)	$\Delta\lambda$ (nm)	I_{th} (mA)	High to low order mode switching	Multi-resonance frequency response	λ_{low} (nm)	λ_{high} (nm)	References
5	300	−22	0.8	No	No	864	…	This work
6	300	−22	1.0	No	No	864	…	This work
7	300	−22	1.5	Yes	Yes	866	857	This work
8	300	−22	1.8	Yes	Yes	866	857	This work
3	300	−8	0.25	No	No	858	…	4
6	300	−8	0.5	No	No	859	…	4
9	300	−8	0.6	No	No	859	…	4
6–7	300	−10	2	Yes	n.a.	945	960	5
10	100	−20	2.5	No	n.a.	…	915	6
10	136	−10	1.0	Yes	n.a.	923	917	6
10	173	0	0.85	No	n.a.	924	…	6

modulation bandwidth reaches 17 GHz with a modulation current efficiency factor (MCEF) of more than 5 GHz/(mA)$^{1/2}$, and then quickly saturates near roll-over. The rate at which the relaxation resonance frequency increases with the square-root of current above threshold, the D-factor, is estimated to be 4.0 GHz/(mA)$^{1/2}$ in the short-wavelength mode regime (with a threshold of 1.5 mA) and 4.5 GHz/(mA)$^{1/2}$ in the long-wavelength mode regime (with a threshold of 4.2 mA). For the 8 μm × 8 μm square aperture oxide-confined VCSEL, the modulation bandwidth reaches 16.5 GHz with an MCEF-factor of 4.5 GHz/(mA)$^{1/2}$. The D-factor is 3.2 GHz/(mA)$^{1/2}$ in the short-wavelength mode regime (with a threshold of 1.8 mA) and is 4.1 GHz/(mA)$^{1/2}$ in the long-wavelength mode regime (with a threshold of 6 mA). We obtained K-factors of less than 0.3 ns, and note that similar VCSEL cavity photon lifetimes are expected for both mode regimes. For both VCSELs, the resonance relaxation frequency saturates only at the L-I rollover bias current indicating a high differential gain for our multiple quantum well active region, while the −3 dB modulation bandwidth reaches a maximum at ∼14 mA for the 7 μm × 7 μm aperture VCSEL and at ∼18 mA for the 8 μm × 8 μm aperture VCSEL. However, current-induced self-heating leads to excessive damping, and, as a result, saturation of the −3 dB modulation bandwidth at a lower current as compared to that for the relaxation resonance frequency. Thus, the −3 dB modulation bandwidth is mostly limited by thermal effects.

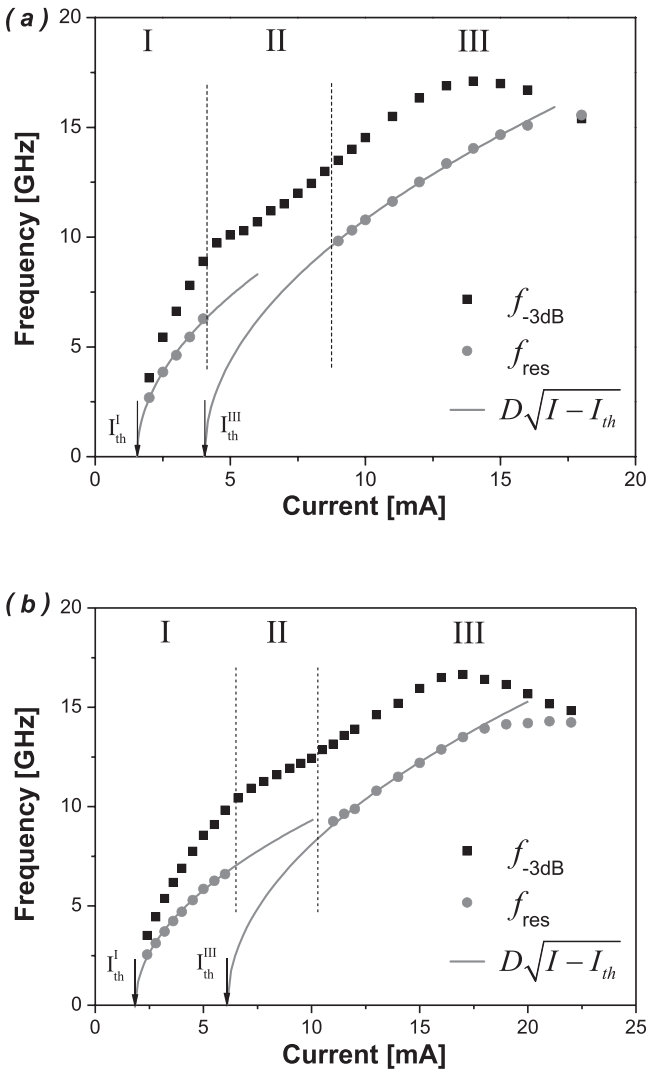

FIG. 4. Extracted-3-dB modulation bandwidth ($f_{-3\,dB}$) and relaxation resonance frequency (f_{res}) as functions of the bias current and the corresponding fits (grey solid lines) as functions of the square-root of bias current above threshold for 7 μm × 7 μm (a) and 8 μm × 8 μm (b) square oxide-confined VCSELs.

A similar multi-resonance frequency response was obtained previously for 960 nm broad-area gain-guided VCSELs operating in a multimode regime,[7] and was explained by differences in mode overlapping levels.[8,9] For the case of uncoupled modes, each transverse mode interacts with its own carrier reservoir, generating its own relaxation resonance frequency. The total response is the incoherent superposition of all resonance peaks. However, the measured modulation response of our VCSELs cannot be evaluated by the direct superposition of the frequency responses with the resonance peaks corresponding to the different mode regimes extrapolated into current region II (grey solid lines). For the case of partially coupled modes, all modes interact with a common carrier reservoir, indirectly coupling among themselves. As a result multiple resonances occur in the total frequency response. For comparison, we note that multimode index-guided VCSELs usually demonstrate a single resonance frequency response. In our case, however, the spectral gap between these distinct modes is about 10 nm, and thus,

one can suggest that the mode competition for the available gain can appear in a two-state lasing regime.

On the other hand, such behavior in a two-state lasing regime can be attributed to sustained self-induced pulsations. In fact, the radio frequency (RF) spectra of a self-pulsating laser include additional harmonics,[10] which can cause the distortion of the modulation response. Note that self-pulsating operation has been previously observed in oxide-confined VCSELs.[11,12] Detailed studies of the RF-spectra and the oscilloscope traces of output optical power under CW operation are underway and will be reported at a later date.

To summarize and conclude, we presented 850-nm VCSELs with a large $\geq$20 nm gain-to-cavity detuning. In our studies, we have observed an anomalous start of lasing via high-order modes with the subsequent switching to the lowest order modes at higher forward bias currents for devices with square oxide aperture sides of length 7 μm and larger. In contrast to the classical VCSEL single-relaxation resonance frequency response for short-wavelength and long-wavelength mode lasing regimes, the small-signal modulation response at currents corresponding to a two-state lasing regime exhibit a more complex modal emission structure. The observed effects must be taking into account for VCSEL applications, where temperature-stable high-speed performance is required.

We acknowledge funding from the Russian Academy of Sciences Presidium Program (No. 24), the Russian Foundation for Basic Research (Grant No. 13-02-12142-ofi_m), and the Deutsche Forschungsgemeinschaft (DFG) via the Sonderforschungsbereiche 787 (Collaborative Research Center 787) at TU Berlin. We thank Connector Optics LLC (St. Petersburg, Russian Federation) for supplying the 850 nm VCSELs.

[1]D. Collins, N. Li, D. Kuchta, F. Doany, C. Schow, C. Helms, and L. Yang, Proc. SPIE **6908**, 690809 (2008).
[2]R. Michalzik, *VCSELs: Fundamentals, Technology and Applications of Vertical-Cavity Surface-Emitting Lasers* (Springer, Berlin, 2013).
[3]D. B. Young, J. W. Scott, F. H. Peters, M. G. Peters, M. L. Majewski, B. J. Thibeault, S. W. Corzine, and L. A. Coldren, IEEE J. Quantum Electron. **29**, 2013 (1993).
[4]L. Y. Karachinsky, S. A. Blokhin, I. I. Novikov, N. A. Maleev, A. G. Kuzmenkov, M. A. Bobrov, J. A. Lott, N. N. Ledentsov, V. A. Shchukin, J.-R. Kropp, and D. Bimberg, Semicond. Sci. Technol. **28**, 065010 (2013).
[5]S. A. Blokhin, N. A. Maleev, A. G. Kuzmenkov, J. A. Lott, M. M. Kulagina, Y. M. Zadiranov, A. G. Gladyshev, A. M. Nadtochiy, E. V. Nikitina, V. G. Tikhomirov, N. N. Ledentsov, and V. M. Ustinov, Proc. SPIE **8276**, 82760W (2012).
[6]C. Degen, I. Fischer, W. Elsaßer, L. Fratta, P. Debernardi, G. P. Bava, M. Brunner, R. Hovel, M. Moser, and K. Gulden, Phys. Rev. A **63**, 023817 (2001).
[7]Y. Satuby and M. Orenstein, IEEE Photonics Technol. Lett. **10**, 757 (1998).
[8]Y. Satuby and M. Orenstein, IEEE J. Quantum Electron. **35**, 944 (1999).
[9]M. S. Torre and H. F. Ranea-Sandoval, IEEE J. Quantum Electron. **36**, 112 (2000).
[10]K. Panajatov, G. Van der Sande, H. Thienpont, and I. Veretennicoff, J. Opt. Soc. Am. B **21**, 1192 (2004).
[11]M. B. Willemsen, A. S. van de Nes, M. P. van Exter, J. P. Woerdman, M. Brunner, and R. Hövel, Appl. Phys. Lett. **77**, 3514 (2000).
[12]A. G. Kuzmenkov, V. M. Ustinov, G. S. Sokolovskii, N. A. Maleev, S. A. Blokhin, A. G. Deryagin, S. V. Chumak, A. S. Shulenkov, S. S. Mikhrin, A. R. Kovsh, A. D. McRobbie, W. Sibbett, M. A. Cataluna, and E. U. Rafailov, Appl. Phys. Lett. **91**, 121106 (2007).